



CONTROL OF SLOW OSCILLATIONS IN THE THALAMOCORTICAL NEURON: A COMPUTER MODEL

W. W. LYTTON,*§ A. DESTEXHE† and T. J. SEJNOWSKI‡

*Department of Neurology, University of Wisconsin, Wm. S. Middleton VA Hospital, 1300 University Avenue, MSC 1720, Madison, WI 53706, U.S.A.

†Howard Hughes Medical Institute, The Salk Institute, La Jolla, CA 92037, U.S.A.

‡Department of Biology, University of California, San Diego, La Jolla, CA 92093, U.S.A.

Abstract—We investigated computer models of a single thalamocortical neuron to assess the interaction of intrinsic voltage-sensitive channels and cortical synaptic input in producing the range of oscillation frequencies observed in these cells *in vivo*. A morphologically detailed model with Hodgkin–Huxley-like ion channels demonstrated that intrinsic properties would be sufficient to readily produce 3 to 6 Hz oscillations. Hyperpolarization of the model cell reduced its oscillation frequency monotonically whether through current injection or modulation of a potassium conductance, simulating the response to a neuromodulatory input. We performed detailed analysis of highly reduced models to determine the mechanism of this frequency control. The interburst interval was controlled by two different mechanisms depending on whether or not the pacemaker current, I_H , was present. In the absence of I_H , depolarization during the interburst interval occurred at the same rate with different current injections. The voltage difference from the nadir to threshold for the low-threshold calcium current, I_T , determined the interburst interval. In contrast, with I_H present, the rate of depolarization depended on injected current. With the full model, simulated repetitive cortical synaptic input entrained oscillations up to approximately double the natural frequency. Cortical input readily produced phase resetting as well.

Our findings suggest that neither ascending brainstem control altering underlying hyperpolarization, nor descending drive by repetitive cortical inputs, would alone be sufficient to produce the range of oscillation frequencies seen in thalamocortical neurons. Instead, intrinsic neuronal mechanisms would dominate for generating the delta range (0.5–4 Hz) oscillations seen during slow wave sleep, whereas synaptic interactions with cortex and the thalamic reticular nucleus would be required for faster oscillations in the frequency range of spindling (7–14 Hz).

Key words: thalamus, inhibition, bursting, spindles, epilepsy.

The thalamus participates in the generation of the rhythms of sleep and is also involved in the pathological spike and wave of absence epilepsy.^{4,42} In the awake state, thalamocortical relay cells show mostly tonic firing. In the early phases of sleep, waxing and waning fast oscillations (spindle waves) are seen; in deep sleep, 0.5–4 Hz delta waves.⁴¹ Absence epilepsy involves 3 Hz slow waves. Slow oscillations occur in isolated thalamocortical cells²² but the frequency is also affected by synaptic input.³⁸ We used computer models to explore the repertoire of slow rhythms of the thalamocortical cell in order to investigate the interplay of intrinsic and extrinsic influences creating these rhythms.

Thalamocortical neurons show two major firing patterns depending on the level of hyperpolarization.²⁰ A low-threshold calcium spike is produced in response to release from hyperpolarized levels; in

contrast, repetitive firing results from current injection from depolarized levels. In addition, a sustained plateau potential has been observed from an initially depolarized level. These *in vitro* firing patterns are of interest because they correspond to *in vivo* patterns underlying the state of the thalamus during sleep, which is characterized by slow rhythms, and the awake state, actively relaying information to the cortex. *In vivo*, two major slow patterns are seen intracellularly: spindling and delta oscillations. Either can be elicited with cortical stimulation depending on the degree of hyperpolarization of the thalamocortical cell.^{31,38} Although it seems likely that the low threshold calcium current underlies both of these slow rhythms, the relative contribution of cellular and network properties to their genesis is not yet fully established.⁴³

The existence of a low-threshold spike in the thalamus was predicted on both experimental and theoretical grounds.^{1,3} The low-threshold spike remained controversial for many years until evidence for a calcium spike was obtained *in vitro*^{20,21} and subsequently shown to be generated by the low-

§To whom correspondence should be addressed.

Abbreviations: EPSP, excitatory postsynaptic potential; IPSP, inhibitory postsynaptic potential; PSP, postsynaptic potential.

threshold calcium current, I_T .⁴⁷ Since this time there has been considerable study of the I_T in thalamic cells^{5,8,13,18} and several computer models have been investigated.^{10,24,27,35,51} During drowsiness or synchronized sleep, the electrophysiological activity of thalamic neurons is dominated by I_T .⁴² This current is normally inactivated during the awake state, but during the transition to sleep, a variety of modulatory inputs from the brainstem, including cholinergic, noradrenergic and serotonergic projections, are reduced, leading to an increase in leak potassium conductances.²⁵ As a consequence, the membrane potential of a thalamocortical cell becomes hyperpolarized and I_T is de-inactivated.

Experiments suggest that both intrinsic neuronal rhythmicity and external driving contribute to the variety of slow oscillations seen physiologically and pathologically. In this paper, we use models to explore to what extent specific ion channels and synaptic inputs contribute to the particular frequencies observed. We first demonstrate that the frequency of oscillation in a thalamocortical neuron model depends on the amount of hyperpolarizing current injection. We then examine the mechanism of this frequency control using phase-plane analysis of minimal models to highlight details of dynamics that are not apparent in the larger, more physiologically realistic, models. Finally, we look at the effects of simulated cortical stimulation on the frequencies in order to demonstrate how cortical input alters different ranges of intrinsic frequencies.

EXPERIMENTAL PROCEDURES

Simulations were run on MIPS Magnum 3000 and SUN Sparcstation 2 computers. The simulations were performed

using modified versions of the programs CABLE and NEURON, the successor to CABLE. Both were developed and implemented by M. Hines.¹⁴ These simulators use a Crank–Nicholson integration scheme that combines excellent stability and second order precision. Approximately 1400 simulations were run to explore various parameter sets and simulation paradigms. Many of these were run in order to establish the validity of the voltage-sensitive channel models by assessing the models behavior under voltage clamp.

Because of the long duration of the simulations and the presence of long interburst intervals with very slowly changing potential, we used a variable time-step in most cases. The time-step was varied between 0.025 ms and 1 ms according to the following algorithm. If the absolute voltage slope remained less than 0.13 mV/ms for 10 ms then the larger time-step would be used. When absolute voltage slope went above 0.13 mV/ms, the shorter time-step was immediately taken. The cutoff point was chosen empirically and produced results nearly identical to those obtained using the smaller time-step consistently. Making the time-step change dependent on m_{Na} did not improve the approximation. Since approximately 2/3 of the duration of a bursting simulation is taken up by the interburst interval, using a long time-step during this period would reduce the simulation time by approximately 60%.

The reconstructed dendritic tree of thalamocortical cell was used for many of the simulations. The morphology for this model was obtained by C-F. Hsiao and M. Dubin using Eutectic's neuron tracing system and provided to us by J. Capowski of Eutectic. This lateral geniculate nucleus neuron may be somewhat larger than other principal thalamic neurons (Fig. 1).^{12,33} The cell was represented in the model by 134 compartments. Soma area was $1275 \mu\text{m}^2$. Membrane capacitance was assumed to be $1 \mu\text{F}/\text{cm}^2$ and longitudinal resistance was $175 \Omega\text{-cm}$. For these simulations, voltage-sensitive channels were present only in the soma. Single compartment models (point neuron) were also used for two purposes. The first was to replicate the standard thalamocortical neuron model developed by McCormick and Huguenard in order to confirm our basic findings.^{16,26} The second was to permit more detailed analysis of the

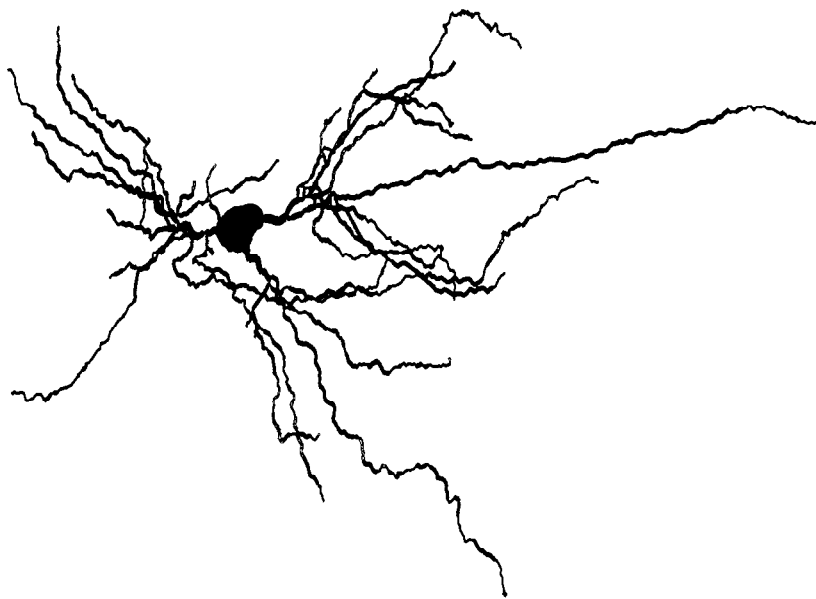


Fig. 1. Morphology of thalamic cell used in compartment model. Lateral geniculate nucleus neuron prepared for light microscopy using the Golgi method and traced with a Eutectics Neuron Tracing System by Drs Hsiao and Dubin (U. Colorado).

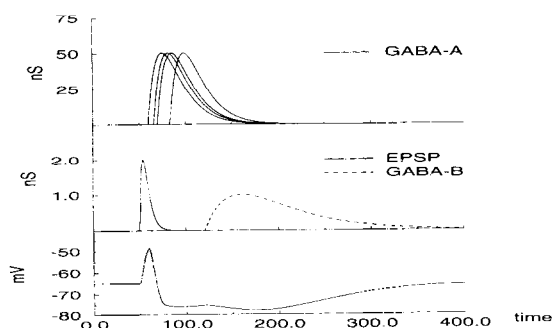


Fig. 2. Complex postsynaptic potential due to cortical shock. Top panel: Four $GABA_A$ conductances at different locations need to be staggered slightly to produce a smooth transition from EPSP to IPSP. Middle panel: Excitatory conductance and $GABA_B$ conductance, identical at each of the four locations. Lower panel: Resulting potential closely matches experimental results.¹²

interaction between injected current, I_T and I_H in a reduced model.

For the current-clamp studies, nine currents were included.^{16,23} Over the course of performing the simulations, these currents were modified as new information was published detailing the kinetics of individual currents. The results described were stable across the various models used. Because most of the data upon which the models were based came from studies done by Huguenard and McCormick, the primary model used was very similar to the McCormick and Huguenard model. The original parameter set used, described in a previous paper,²⁴ was modified by the replacement of potassium channels with those obtained from studies in thalamocortical cells: I_{Kd} , I_{K2} and I_A .^{15,17} Corresponding channels from the previous model, including I_M , were eliminated. Various I_T parameters, taken from a variety of sources, were used, as described in a previous paper.²⁴ The other major difference from the McCormick and Huguenard model lay in the use of multiple calcium elimination mechanisms (Ca^{2+} -ATPase, Na^+/Ca^{2+} exchange and diffusion) instead of first-order elimination in most parameter sets. A first-order calcium elimination scheme was also tried and gave similar results. As noted, qualitative results were the same when checked using an implementation of the McCormick and Huguenard model.

Characteristic values for channel density parameters were g_{Na} 1.0, g_{NaP} $2 \cdot 10^{-4}$, g_{Kd} 0.05, g_A 0.05, g_{K2} $2.8 \cdot 10^{-3}$, g_H $1.8 \cdot 10^{-3}$ S/cm² and p_T $2 \cdot 10^{-3}$, p_L $8 \cdot 10^{-5}$ cm/s. The leakage conductance was $5 \cdot 10^{-5}$ S/cm² except in the soma where it was adjusted to compensate for resting currents to provide a resting membrane potential of -65 mV using a leakage reversal of -100 mV ($1.44 \cdot 10^{-3}$ S/cm² here). In this case, the apparent input impedance of the cell was 50 M Ω with membrane time constant of 4.7 ms. In the absence of I_H , the input impedance was 66 M Ω with a 6.6 ms membrane time constant. These values varied widely with different parameter sets due to dependence of overall conductance on the amount of inward current through voltage-sensitive channels at rest. The values were generally within the range observed in the lateral geniculate nucleus in cat and rat.^{6,7}

Over the course of this project, we used about 10 distinct parameter sets to assess the dynamics of the thalamocortical neuron. The parameters were changed when new information came to light permitting a more accurate version of a particular ion channel to be included. Additionally, we checked our results using the parameters of McCormick and Huguenard, whose model of thalamocortical cell currents is the most complete available.¹⁶ Since we also analysed basic mechanisms of the oscillation in detail, we expect that our

results are not dependent on the details of any particular parameter set.

With the full neuronal morphology represented with 134 compartments, 1 s of simulated time took about 4 min to run without graphics on a SUN Sparcstation 2 computer.

Cortical stimulation was simulated by matching intracellular voltage traces from *in vivo* intracellular study of thalamocortical neurons (Fig. 2).³⁸ Both excitatory and feedforward inhibitory synapses were located at four sites about $100 \mu\text{m}$ out on the dendrites. The feedforward inhibitory postsynaptic potential (IPSP) followed the excitatory postsynaptic potential (EPSP) at about 30 ms for $GABA_A$ and 50 ms for a 300 ms duration $GABA_B$ response, corresponding to the data. We found that activating the four $GABA_A$ inputs at slightly different time intervals following the initial EPSP was necessary to obtain the smooth transition between EPSP and IPSP observed electrophysiologically. This alteration was only required to improve the appearance of the postsynaptic potential (PSP) since the response of the thalamocortical neuron was identical with or without it.

RESULTS

Hyperpolarization, whether by current injection or synaptic activation, served to slow down the frequency of bursting. Excitatory synaptic stimulation by simulated cortical shock would speed up bursting but would not slow it down. Purely inhibitory synaptic stimulation would, however, slow down bursting. Individual bursts had a consistent duration of about 30 ms. One to three sodium spikes would generally occur on top of the burst with a frequency of 300–400 Hz which would decrease during the course of the burst.

Brief hyperpolarization can produce sustained oscillation

Rhythmic bursting in thalamocortical neurons depended on the interaction between I_T and I_H . Because of the presence of this calcium current, thalamocortical neurons showed a burst of spikes upon release from hyperpolarization. With most parameter sets, this burst was followed by an oscillation, in some cases sustained (Fig. 3). This was due to the fact that the depolarization during the burst turned off inward currents through deactivation of I_H and inactivation

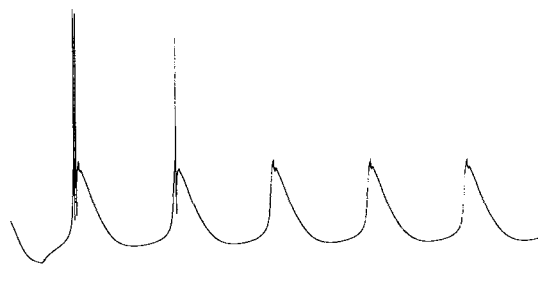


Fig. 3. After release from a brief hyperpolarizing pulse, thalamocortical cell model shows persistent oscillation. Model neuron is hyperpolarized for 50 ms with a -0.08 nA current pulse. Scale: 200 ms, 25 mV.

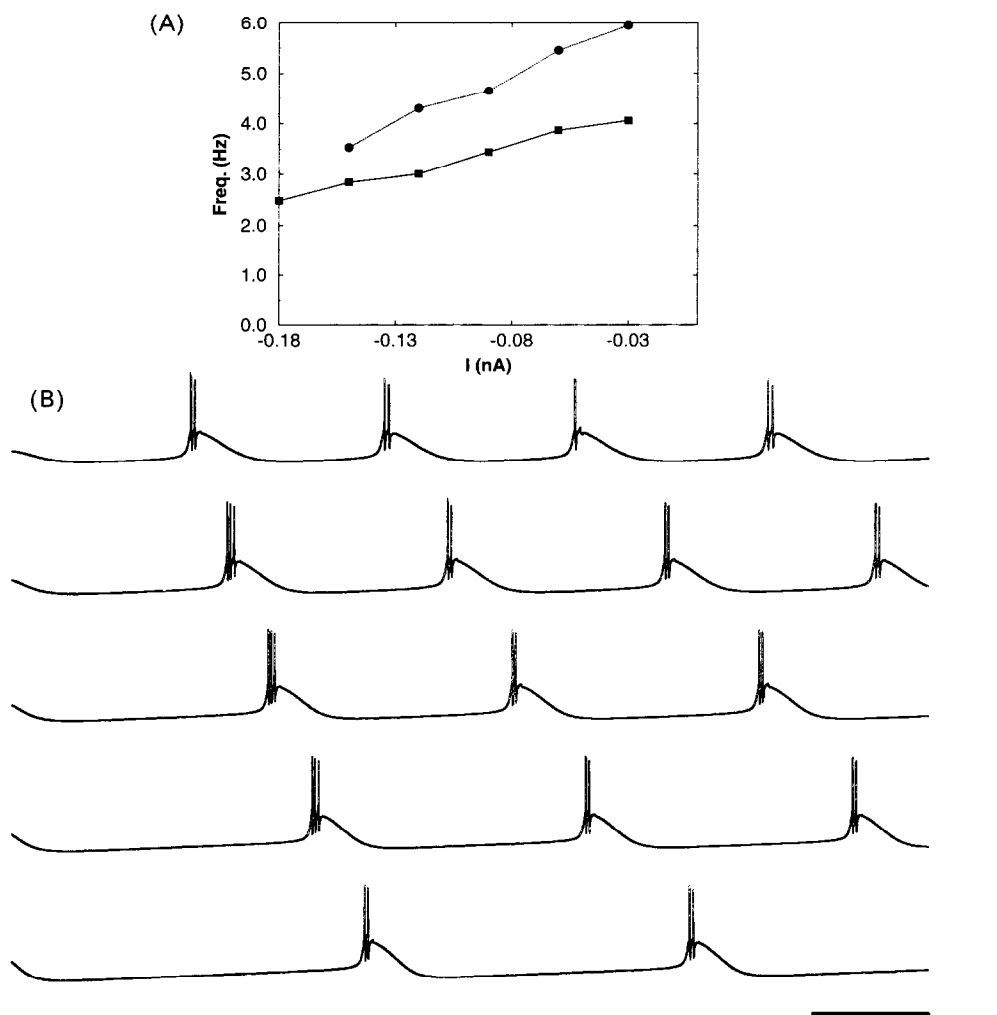


Fig. 4. (A) Increasing injection of negative current reduces rate of oscillation. Current increase from -0.3 nA to -0.18 nA gives decreasing frequency of bursting. (B) Voltage traces correspond to upper curve in A. Scale: 100 ms, 100 mV.

of I_T , leading to a subsequent hyperpolarization that prepares for the next burst.²⁸

In general, increasing I_T would increase the strength of bursting and make it more likely that a single input would be followed by repeated bursts. At high enough I_T density, the resting membrane was unstable and the model would oscillate spontaneously.

Bursting frequency is slowed by negative current injection

The bursting frequency could be controlled by altering the amount of hyperpolarizing current injected into the soma (Fig. 4). Increasing the negative current injected would invariably slow the frequency of bursting, but the duration of the burst was not affected by the current injection. Therefore, the oscillation frequency was determined by the duration of the interburst interval. This is comparable to the control of Hodgkin–Huxley sodium action potentials by positive current injection, in that change in the

interspike interval, not spike duration, determines frequency.

The lowest frequency possible occurs at the point when the current injected overwhelms the ability of I_H to repolarize the neuron to the point where a low-threshold calcium spike can occur. Therefore, increases in I_T or I_H generally permitted lower frequency oscillations. With the models that we used, the lowest frequencies were about 1 Hz. The highest frequency obtained with a particular model could be obtained with the response to a brief hyperpolarization or, in the case of spontaneously oscillating cells, would occur at the resting potential with no stimulation. Depolarization generally produced repetitive sodium spikes rather than burst firing. The fastest burst frequency obtained with the models we used was 9 Hz but most models would not oscillate at more than 6 Hz, consistent with what has been shown experimentally (Fig. 7 in Crunelli *et al.*⁶). Increased I_T in our model decreased the maximal frequency by providing larger bursts that led to more pronounced

interburst hyperpolarization. Although increased I_H increased oscillation frequency under hyperpolarized conditions,²⁶ the increase would not effect the maximum possible frequency.⁵¹

Similar frequency control was obtained by simulating the alteration in potassium conductance that would occur with changes in modulatory transmission from brainstem sites.²⁵ Increasing a leak potassium conductance produced slowing of oscillation. This differs from hyperpolarization introduced by current injection since there is an associated increase in membrane conductance and since the amount of outgoing current varies depending on the membrane potential of the neuron. Due to the large driving force used (35 mV from the resting level to E_K), the change of membrane conductance was not significant relative to baseline. The voltage-dependency of current also had very little effect since voltage excursion is relatively small during the interburst interval (see below).

Two mechanisms of frequency control by current injection

Over many parameter sets, bursting frequency slowed with increasing hyperpolarization. Two different patterns were found associated with the response to negative current injection in a wide variety of parameter sets. In most cases, increasing negative current injection caused greater hyperpolarization during the interburst interval, with the depolarizing slope and the burst threshold remaining fairly constant. Therefore, the degree of hyperpolarization largely determined the amount of time required to reach threshold. In other cases, the potential during the interburst interval did not increase with increasing negative current. Since the complexity of our full models did not permit direct analysis of these different patterns, we turned to highly simplified models to assess this further. Note that these are simply "models of the models" and not meant to directly model the physiology.

We were able to reproduce these two patterns using highly simplified models that included only currents fundamental to the rhythm. One pattern could be obtained by using I_T alone in a point neuron while the other was obtained using both I_T and I_H together. In both cases, the interburst interval was dominated by the quasi-steady state that occurred as opposing currents balanced. The difference in the location of this balance point was due to the fact that, in the I_T -dominated pattern, the dominant current turned on during the depolarizing interburst interval (since $m_{\infty T}$ increases with increasing potential) while in the I_H -dominated pattern, the dominant current turned off during this period.

With only I_T present, the more common pattern was seen: different potentials during the interburst interval with similar slopes (Fig. 5). Superimposing voltage trajectories from a fast-oscillating model

(dotted line) and a slow-oscillating model (solid line), obtained with differing amounts of negative current injection, illustrates that the slow model (greater negative current and prolonged interburst interval) was associated with more hyperpolarization (Fig. 5 top). In the phase plane, the ascending trajectories for the different currents are illustrated against voltage during the depolarizing phase of the two interburst intervals (Fig. 5 bottom). At the nadir of the interburst interval, where the trajectories begin, the increasing positive leakage current (no symbol) approximately matched the current injection (triangles) causing voltage to reverse direction. I_T made a small contribution due to residual current not inactivated during the course of the preceding burst.

From this nadir, both slow and fast trajectories are determined by the small, approximately equal, total currents that stay fairly constant during depolarization due to the near match between increasing inward I_T and increasing outward leakage current. This match reflected the match between the nearly linear $m_{\infty T}$ curve in the subthreshold range with the perfectly linear leak current. Though the driving force for I_T was decreasing during this depolarization, the decrease was minimal so far from the Ca^{2+} reversal potential. (The concept of a Ca^{2+} reversal potential is a fair approximation at this voltage although the Goldman-Hodgkin-Katz equation was actually used to calculate current.) Threshold for a regenerative I_T was reached at about -80 mV in both cases, causing I_T to deviate abruptly from linearity off the left side of the phase plane (not shown).

When a sufficient density of I_H was added to the thalamocortical cell model, quite a different pattern was observed (Fig. 6). Now there were two stages to the interburst interval: an initial depolarizing stage followed by a quasi-equilibrium. In contrast to the previous case, now the faster model (dotted line), associated with less negative current injection, showed the more hyperpolarized potential (Fig. 6 top). On the phase plane (Fig. 6 bottom), the total current has been magnified 100 times to better show the difference between the two currents. The initial depolarizing stage extended from the nadir up to the potential of the quasi-equilibrium. The quasi-equilibrium occurred at the voltage where the activation curve for I_H turns sharply downward. Since further depolarization decreased I_H , depolarization stalled at this point.

The duration of both stages of the interburst interval was shorter in the faster model. This difference could be traced back to the equilibrium point at the voltage nadir. Since less current was being injected into the faster model, less opposing current was required to equal it and produce equilibrium. In the faster model, this point was reached at a more depolarized voltage which was associated with less opposing leak current. The rapid hyperpolarizing plunge does not substantially activate I_H , so the difference in driving force (20% in this case) accounts

almost entirely for the difference in current. This was demonstrated by noting that a line drawn through the two initial I_H values intersects 0 current nearly at the E_H of -40 mV (the slope gives g_H). Leakage conductance (g_{leak}) is larger (greater slope) than g_H . Relative to I_H , I_{leak} makes a greater contribution at the equilibrium current in the slow model. With depolarization, I_{leak} grows in opposition to increasing I_H . In the first stage of the interburst interval, the total current for the two models was roughly comparable and the difference in duration was largely due to the difference in the voltage distance to be traversed from the nadir to the quasi-equilibrium. In the quasi-equilibrium stage, the reduced interburst interval duration of the faster model was due to the 75% greater total current contributed by the increased I_H present due to the aforementioned differing conditions at equilibrium.

Cortical stimulation can entrain thalamocortical neurons

The initial EPSP from the simulated cortical shock was sufficient to produce a low-threshold calcium

spike in the hyperpolarized model. Because of this, simulated repetitive cortical shock was able to entrain the oscillation frequency to higher but not to lower values. In general, the frequency could be approximately doubled with driving (Fig. 7), as has been seen experimentally (Steriade *et al.*, Fig. 3³⁸). With faster attempted driving, the duration of the interstimulus interval was not sufficient to allow recovery of I_T . Therefore, the value of τ_{hT} determined the fastest frequency of driving. Using a larger initial EPSP, a burst-like appearance was seen due to sodium spikes riding on top of the EPSP itself. These could be driven to higher frequencies since they did not involve the low-threshold calcium spike. Driving was then limited by the duration of the feedforward IPSP which interfered at high frequency with the subsequent EPSP.

Using this stimulation, slowing of oscillation was not possible. Since the strength of the feedforward IPSP was sufficient to trigger a low-threshold calcium spike, this rebound burst would occur before the next stimulated burst. Thereafter a doublet rhythm was produced with a large rebound low-threshold calcium

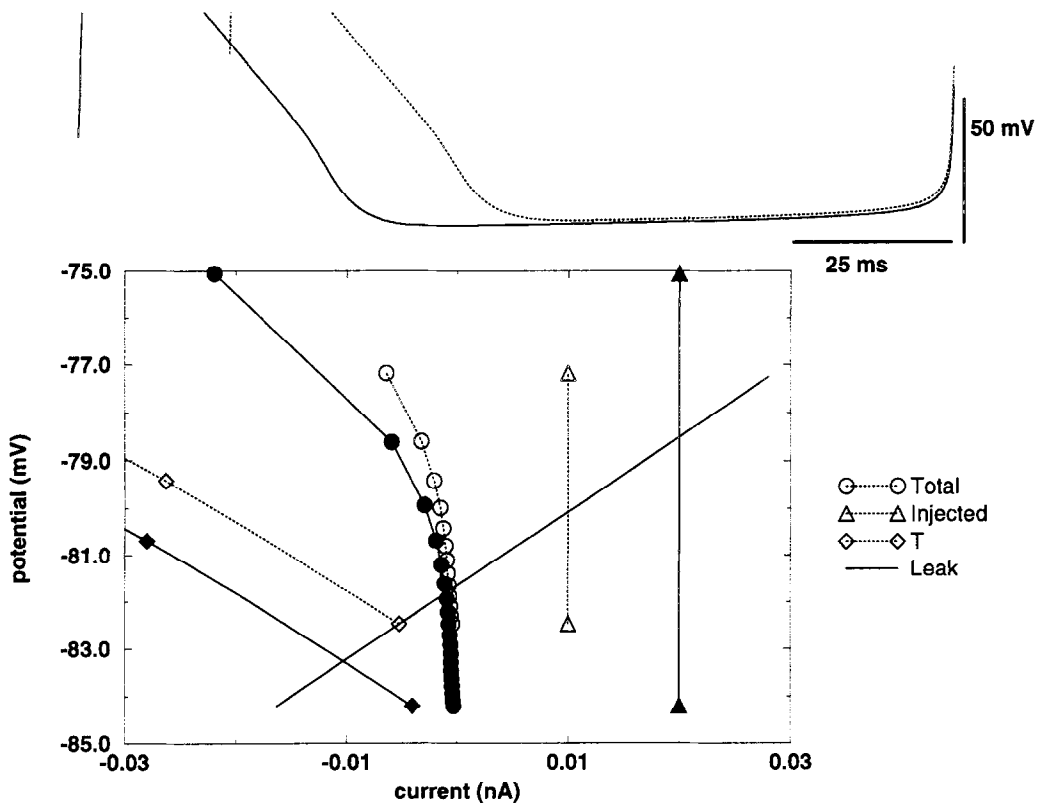


Fig. 5. Phase plane analysis of current injection control of oscillation frequency in point neuron model with I_T (the low-threshold calcium channel) alone. Top: One cycle of oscillation is compared between a fast-oscillating model (dotted line) and a slow-oscillating model (solid line). Burst peaks are truncated. Bottom: The ascending trajectories of the interburst interval are examined in a phase-plane representation. Each current in the model is compared for the fast-oscillating (dotted line) and slow-oscillating models (solid line). The currents are distinguished by a symbol at the endpoints of the trajectory segment given. No symbol is used for the leak current which is identical for the two models. For total current, the symbols are used to mark time points (circles are 4 ms apart). Time points for other trajectories can be obtained by drawing a line horizontally from a time point to that trajectory. Depolarization is caused by positive current due to I_{leak} from -85 to -82 mV ($E_{rev_{leak}}$) and I_T thereafter.

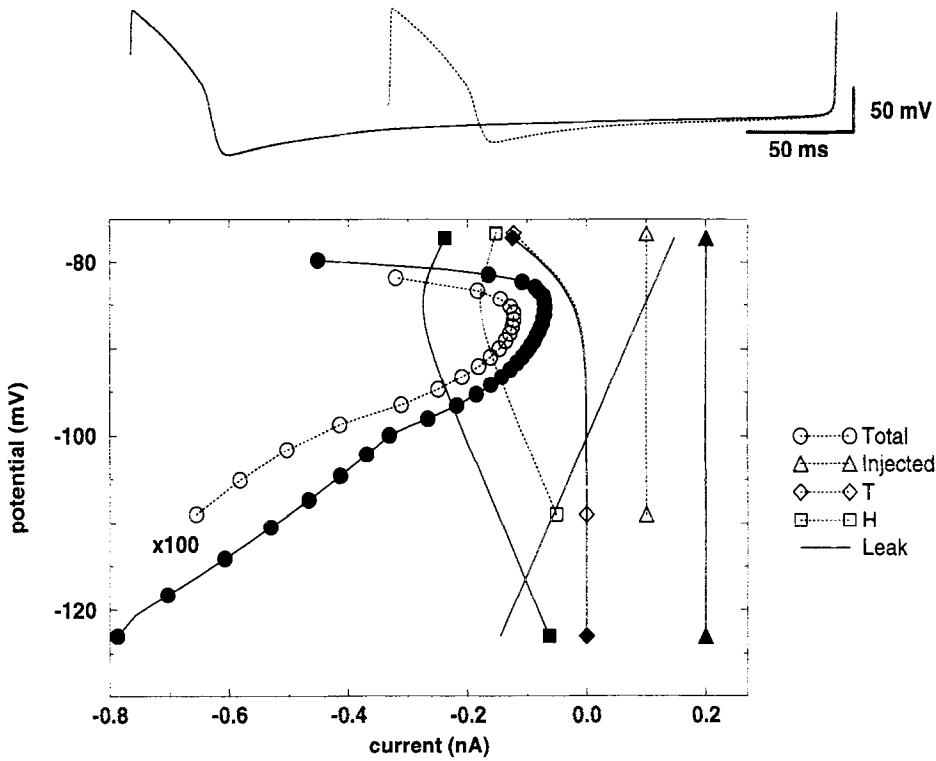


Fig. 6. Phase plane analysis of current injection control of oscillation frequency in point neuron model with I_T (the low-threshold calcium channel) and I_H (the anomalous rectifier). Top: One cycle of oscillation is compared between a fast-oscillating model (dotted line) and a slow-oscillating model (solid line). Bottom: Phase-plane of ascending trajectories of the interburst interval. As in Fig. 5, currents are compared for the two cases and marked by symbols. In this case, the time marks for the total current are 8 ms apart.

spike followed by a smaller stimulated EPSP/low-threshold calcium spike (Fig. 8).

Cortical stimulation does not necessarily lead to an immediate low-threshold calcium spike, even at hyperpolarized potentials.³⁸ The relative influence of the direct cortical EPSP and the feedforward IPSP may differ between cells depending on the amount of divergence from cortical pyramidal cell to thalamic interneurons and the amount of convergence from the latter to a single thalamocortical neuron. There-

fore we assessed the effect of frequency entrainment in the absence of the initial EPSP. The isolated feedforward IPSP could not speed up bursting since the degree of baseline hyperpolarization did not leave enough I_T non-deactivated for further hyperpolarization to produce a low-threshold calcium spike. Therefore higher frequency IPSPs simply lead to temporal summation. This stimulation was able to slow down bursting to a limited extent (Fig. 9A). Attempting further slowing produced doublet burst-

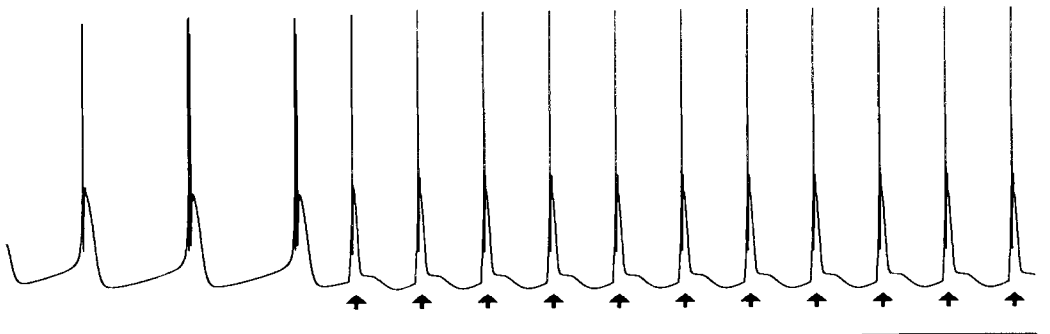


Fig. 7. Entrainment of thalamocortical model neuron. Intrinsic oscillation at 3.2 Hz produced by hyperpolarization is frequency entrained upward to 5.2 Hz by repetitive cortical synaptic input at this rate (arrows). Cortical EPSP is followed by feedforward inhibition. Scale: 500 ms, 20 mV.

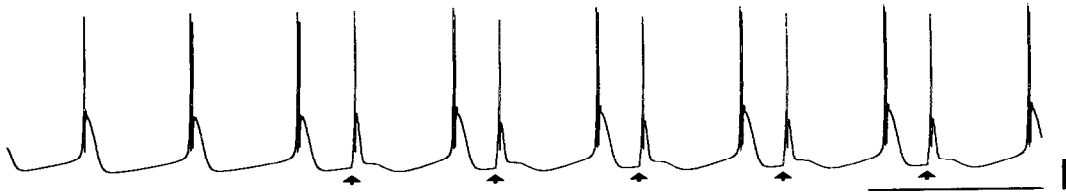


Fig. 8. Simulated cortical stimulation at a frequency (2.4 Hz) slower than the intrinsic oscillation (3.2 Hz) produces burst doublets consisting of a large rebound low-threshold spike followed by a smaller stimulated EPSP/low-threshold spike. Scale: 500 ms, 20 mV.

ing (Fig. 9B). The prolonged hyperpolarization results in the twin burst occurring at a slightly higher frequency than is seen without the stimulation.

Cortical stimulation can change oscillation phase

In addition to frequency alteration with cortical stimulation, a single simulated cortical shock during the oscillation could readily reset the phase (Fig. 10), similar to the effect of brief current injection *in vitro*³⁶ or cortical stimulation *in vivo*.³⁸ Phase resetting would occur equally well with stimulation anywhere in the cycle. Stimulation would produce a low-threshold calcium spike which would determine the subsequent phase. Phase resetting was equally effective with the feedforward IPSP alone. In this case the low-threshold calcium spike that followed the IPSP would initiate the new phase.

DISCUSSION

We have shown how intrinsic properties of thalamocortical cells can interact with external influences to determine the bursting frequency of these cells. In some cases, these external influences will be sustained, as in the activity of modulatory neurons projecting from the brainstem. In other cases, the inputs are brief, as in synaptic activation from cortex, but can

nonetheless, through phase resetting, produce a long-lasting influence. In either case, the response of the neuron to stimulation can only be understood in the context of the many interacting ion channels that give the thalamocortical cell its complex dynamics.

Current injection and hyperpolarization

We demonstrated frequency control within a limited range using constant current injection. Using various parameter sets, we generally obtained frequencies in the 1–6 Hz range. In contrast, Wang⁵¹ demonstrated frequencies up to 12 Hz with current injection. In comparison with Wang's model, our model contains additional potassium currents as well as the L calcium current in a full multi-compartment model. The inability to obtain the higher frequencies in our model may be due to the greater impedance load provided by the full multi-compartment simulation. This impedance load may be underestimated by our model and might explain the remaining discrepancy with the slower maximum frequencies obtained experimentally.

Although negative current injected into a neuron always produces an initial hyperpolarization, its overall effect depends on the response of voltage-sensitive channels that can respond by augmenting or opposing the current. Since these additional currents are

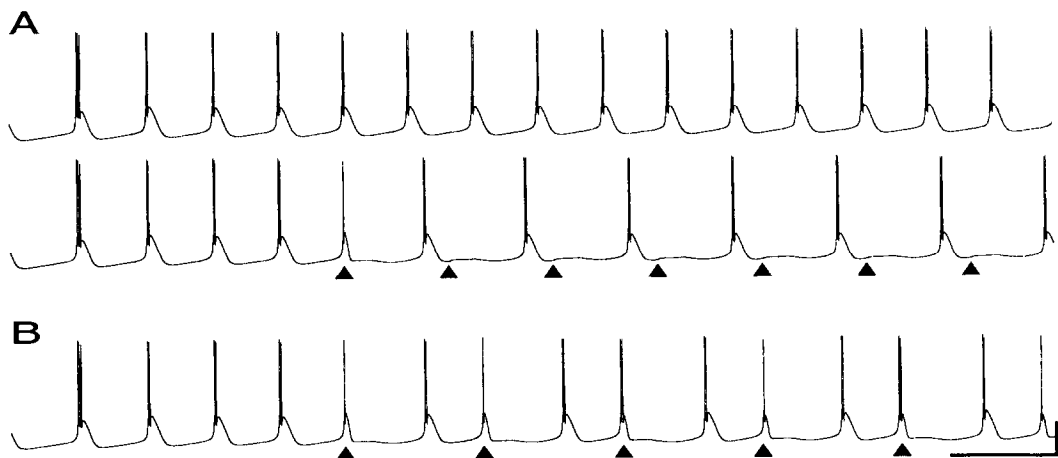


Fig. 9. (A) Reduction of 6.4 Hz oscillation (upper trace) with 4.0 Hz repetitive feedforward IPSP stimulation at arrowheads produces downward frequency entrainment (lower trace). (B) Attempt to reduce frequency still further to 3.0 Hz fails to produce entrainment but produces doublet bursting. The second burst precedes the stimulation slightly; the apparent coincidence is fortuitous. Scale: 250 ms, 40 mV.

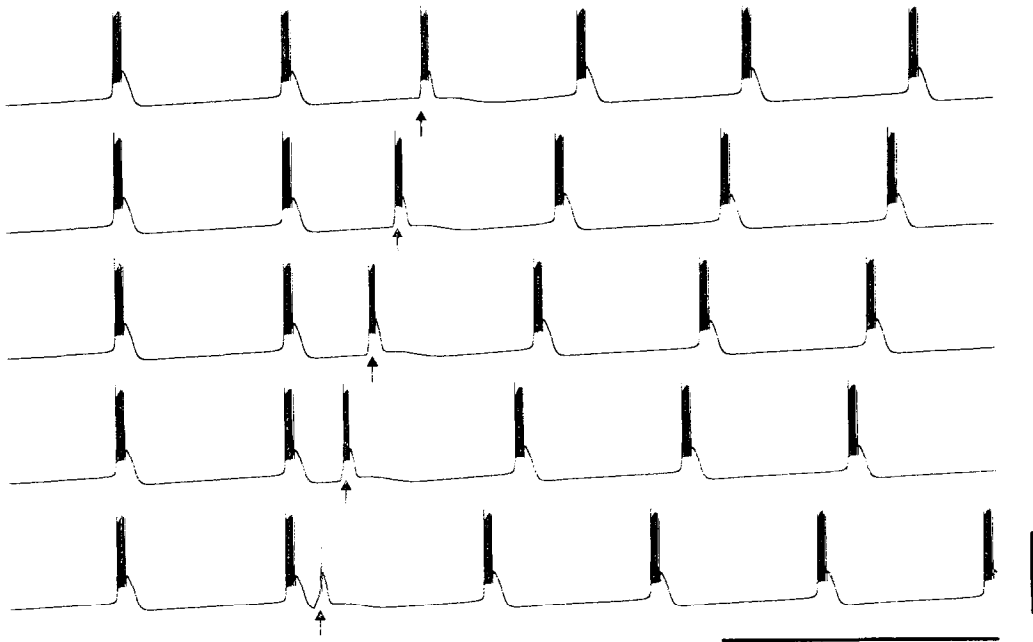


Fig. 10. Phase entrainment with simulated cortical shock. Single shock is given at arrow in each case. Scale: 500 ms, 100 mV.

non-linear, the neuron can behave differently for different voltage ranges. For example, the anomalous rectifier, I_H , opposes hyperpolarization, producing a "sag" in the response of a cell to a constant hyperpolarizing current. In our thalamocortical cell model, we studied two conductance responses in detail: I_T and I_H .

I_T shows both activation and inactivation. In the hyperpolarized voltage range important for controlling bursting rate, I_T gradually de-inactivated following the burst. Although inactivation had a long associated time-constant (τ_h), the value was so far from steady-state (h_∞) that it increased relatively quickly. Steady-state activation (m_∞) had a low value in this voltage range, and activation therefore contributed less to the total permeability ($p \cdot m^2 \cdot h$). Initial hyperpolarization was almost entirely determined by passive properties since the inward leakage current gradually increased with hyperpolarization until it matched the injected current. Having reached the full degree of hyperpolarization, the activation of I_T then determined the pattern of the depolarization. In this case the slow increase in I_T was nearly matched by the decrease in leakage current caused by the gradually reducing driving force. This balance is to be expected in an increasing current in its subthreshold range opposed by a linearly increasing current whether the latter is the leakage current or a subthreshold outward current. Until such a current reaches an inflection in its activation (by definition a threshold) which causes it to become self-regenerative, it will find a balance such that its effect on voltage will be limited by the opposing current. This would suggest that an increased I_T density would give an increased rate of

oscillation, as the current balance will then occur at higher total inward current allowing more rapid depolarization and a shorter interburst interval. However, in the full model, the more exuberant burst associated with increased I_T can activate a variety of other channels that increase the interburst hyperpolarization to produce slowing.

On the other hand, the inflection of the steady-state curve for I_H served as a brake to further depolarization rather than as a threshold leading to a self-regenerating current. Where rate control in the I_T -only model was produced by a balance between inward and outward current, here it is determined by the conditions at equilibrium (zero total current) as the voltage turns upward. The equilibrium occurs when there is sufficient leakage current to oppose the current injection. At this point inward current increases with I_H until the resultant depolarization produces opposition from I_{leak} resulting in a local maximum of total inward current (the starting point on the phase plane). The smaller τ_h at the more hyperpolarized potential permits a more rapid increase in I_H and consequent greater current. However, this is not enough to make up for the opposition from I_{leak} .

Brainstem modulatory control over oscillation rate

A variety of brainstem modulatory projections influence thalamocortical neurons.²⁵ In general these produce prolonged increases in potassium currents which may, in some cases, be non-voltage-dependent leak currents. Through alteration of the degree of hyperpolarization, these projections could control the frequency of oscillation, as has been previously

noted.²⁵ Though the ability of these ascending systems to shift the thalamus between slow-wave and fast-spiking states has been emphasized, we found that these influences will also be important in determining the rates of slow oscillations. This might aid in changing between the relatively rapid rate of the spindling characteristic of human stage II sleep, and the delta frequencies seen in deep sleep and in absence epilepsy.

Cortical control over oscillation in anterior thalamus

The anterior thalamus is unusual in that it does not have an associated thalamic reticular nucleus.⁴⁶ Therefore, the intrinsic interneurons, if present, provide all of the GABAergic input into the thalamocortical neurons there. While most thalamic nuclei have both interneurons and inhibitory feedback from the reticular nucleus, there are also examples where reticular nucleus is present and interneurons are absent.³⁴ Experimentally, cortical input to thalamus is assessed by electrical shock to the underlying white matter which will also produce cortical activation as well as antidromic effects. This paradigm is expected to give a near maximal excitation producing a complex PSP involving both the direct EPSP and feedforward IPSPs. Analysis of the IPSP has suggested that it involves two locations of GABA_A receptors as well as GABA_B receptors. We were able to model the resulting waveform empirically by staggering the arrival of the GABA_A input.

Naturally occurring cortical inputs would presumably involve patterned activation of projections that could result in different proportions of excitatory and inhibitory input. Therefore, we assessed both the mixed PSP and the IPSP alone. In the case of the mixed PSP, the initial EPSP played the critical role in triggering a low-threshold calcium spike from the hyperpolarized potential. The oscillation frequency could be increased considerably using this input. This PSP was not effective in slowing down frequency of firing, however, since the neuron would rebound from the inhibitory portion before the next cycle. A longer IPSP would permit this slowing to occur since the IPSP would maintain the hyperpolarized state until the next EPSP occurred. The range of slowing across which this would be effective depended on the duration of the IPSP.

The IPSP alone was able to slow oscillation. Again, the duration of the IPSP is the limiting factor on how much slowing is possible. As seen in Fig. 9B, an IPSP insufficiently prolonged for the cycle period will result in a subsequent burst before the next cycle is initiated. Additionally, if the strength of the IPSP is insufficient relative to the oscillatory drive of the cell (determined by the density of I_T and I_H), even a prolonged IPSP may not be able to prevent an escape burst of this sort.

While frequency entrainment was somewhat limited, phase entrainment was very robust whether the mixed PSP or just the IPSP was used. Regardless of

where in the cycle the stimulation was given, a new phase could be initiated at that point. Though the EPSP component could not produce a full burst early in the cycle, the subsequent IPSP would delay the occurrence of the next burst so as to shift the phase. In the absence of the IPSP, the EPSP would only be able to set phase when it occurred during the latter part of the cycle where it could trigger a low-threshold calcium spike.

The duration of the feedforward IPSP in our model is approximately 250 ms. This is also seen in thalamic areas that receive projections from reticular nucleus.¹⁹ This period corresponds to a frequency of approximately 4 Hz. Since the ability of cortical stimulation to provide frequency and phase control is partly dependent on this duration, there may be matching between the frequency of oscillation and the form of cortical input utilized to control it.

Insights into the mechanisms of thalamic oscillations

The present model confirms that the interplay of I_T and I_H generates slow oscillations in thalamocortical neurons, as suggested from intracellular recordings *in vitro*.^{29,37} Different models of thalamocortical cells have been proposed.^{10,24,26,48,50} Although they used different equations and activation functions, they have all confirmed the genesis of slow oscillations on the basis of an interaction between I_T and I_H . Unlike previous models of thalamocortical cells, which included only a single compartment, the model we studied included a full dendritic tree. The dendrites provide an additional impedance load that would be expected to decrease the ability of the model to sustain oscillations. The presence of the oscillation in this context lends further credence to the validity of the hypothesis of slow oscillations as being generated by I_T and I_H . This additional impedance would also be expected to reduce the maximum frequency of the oscillations. In fact our maximum frequency was significantly below that seen in previous models.⁵⁰ We may still be underestimating the impedance load of the dendritic tree. This is a possible explanation for why our maximal frequencies remain slightly higher than those seen experimentally.

Intracellular recordings of thalamocortical cells in decorticate cats *in vivo*^{9,31} have not shown involvement of IPSPs in low-frequency rhythmic oscillations. In the present model, we found a gradual decrease in oscillation rate with hyperpolarization. This is consistent with the hypothesis that slow thalamic oscillations between 1 to 6 Hz might be due primarily to mechanisms intrinsic to thalamocortical cells, in agreement with other models.^{10,24,26,48,50} We predict that for frequencies in this range the role of the cortex will be to set the phase of oscillation but not to determine the frequency.

On the other hand, intracellular recordings of thalamocortical cells during spindle rhythmicity show a powerful involvement of the reticular nucleus, both

in vivo^{39,40} and *in vitro*.⁴⁹ The present model shows that in the absence of synaptic inputs, the thalamocortical cell is not capable of sustaining oscillations at this frequency.³⁹ This is consistent with experimental results,⁴⁹ as well as with a model of spindling proposed previously,¹¹ in which the 8–10 Hz frequency of spindling was imposed by IPSPs from reticular nucleus cells. This previous model also predicted that the exact frequency of spindles depends critically on the decay of GABAergic IPSPs from the reticular nucleus cells. The data from the present model are consistent with these previous studies.

In addition to the waxing and waning envelope of spindle oscillations, there exist other modulatory influences on low-frequency thalamocortical oscillations. A slow oscillation of cortical origin, described recently,^{44,45} potentiates the grouping of thalamic oscillations (spindle, delta or fast oscillations) in recurring sequences at a frequency of 0.3–1 Hz. While these slow cortical waves might participate in the waxing and waning envelope of spindle oscillations, waxing and waning has also been observed in thalamic slices which lack cortical inputs.⁴⁹ We found no evidence for a mechanism that would allow cortical EPSPs to extinguish the oscillatory behavior in thalamocortical cells, therefore the present model is consistent with a non-cortical origin of the envelope. The

possibility of a waxing and waning influence intrinsic to thalamocortical cells^{25,30} was supported by a previous model.^{10,11}

CONCLUSION

The present model predicts that intrinsic mechanisms dominate to produce oscillations in the delta range (0.5–4 Hz) in thalamocortical cells. Although these cells have no intrinsic mechanisms for generating faster oscillations in the range of spindling (7–14 Hz), we found that they can be easily entrained to these frequencies. These data support the view that synaptic inputs from the cortex and thalamic reticular nucleus are involved in determining the phase and frequency of oscillations in thalamocortical cells. However, the effects of inter-mixed feedback between thalamocortical, reticular and cortical neurons cannot be predicted intuitively: computational network models will be needed to further explore the range of possibilities.

Acknowledgements—We would like to thank the two anonymous reviewers for many helpful comments. This research was supported by the Epilepsy Foundation of America, NINDS and the Veterans Administration (WWL), by HHMI (AD) and by NIMH (TJS).

REFERENCES

1. Andersen P. and Andersson S. A. (1986) *Physiological Basis of the Alpha Rhythm*. Appleton-Century-Crofts, New York.
2. Andersen P., Gillow M. and Rudjord T. (1966) Rhythmic activity in a simulated neuronal network. *J. Physiol., Lond.* **185**, 418–428.
3. Andersen P. and Rudjord T. (1964) Simulation of a neuronal network operating rhythmically through recurrent inhibition. *Nature* **204**, 289–290.
4. Avoli M., Gloor P., Kostopoulos G. and Naquet R. (1990) *Generalized Epilepsy*. Birkhäuser, Boston.
5. Coulter D. A., Huguenard J. R. and Prince D. A. (1989) Calcium currents in rat thalamocortical relay neurones: kinetic properties of the transient low-threshold current. *J. Physiol., Lond.* **414**, 587–604.
6. Crunelli V., Kelly J. S., Leresche N. and Pirchio M. (1987) The ventral and dorsal lateral geniculate nucleus of the rat: intracellular recordings *in vitro*. *J. Physiol., Lond.* **384**, 587–601.
7. Crunelli V., Leresche N. and Parnavelas J. G. (1987) Membrane properties of morphologically identified x and y cells in the lateral geniculate nucleus of the cat *in vitro*. *J. Physiol., Lond.* **390**, 243–256.
8. Crunelli V., Lightowler S. and Pollard C. E. (1989) A T-type Ca^{2+} current underlies low-threshold Ca^{2+} potentials in cells of the cat and rat lateral geniculate nucleus. *J. Physiol., Lond.* **413**, 543–561.
9. Curro Dossi R., Nunez A. and Steriade M. (1992) Electrophysiology of a slow (0.5–4 Hz) intrinsic oscillation of cat thalamocortical neurones *in vivo*. *J. Physiol., Lond.* **447**, 215–234.
10. Destexhe A., Babloyant A. and Sejnowski T. J. (1993) Ionic mechanisms for intrinsic slow oscillations in thalamic relay neurons. *Biophys. J.* **65**, 1538–1552.
11. Destexhe A., McCormick D. A. and Sejnowski T. J. (1993) A model for 8–10 Hz spindling in interconnected thalamic relay and reticularis neurons. *Biophys. J.* **65**, 2474–2478.
12. Guillery R. W. (1966) A study of Golgi preparations from the dorsal lateral geniculate nucleus of the adult cat. *J. comp. Neurol.* **128**, 21–50.
13. Hernandez-Cruz A. and Pape H. C. (1989) Identification of two calcium currents in acutely dissociated neurons from the rat lateral geniculate nucleus. *J. Neurophysiol.* **61**, 1270–1283.
14. Hines M. L. (1989) A program for simulation of nerve equations with branching geometries. *Int. J. Biomed. Comp.* **24**, 55–68.
15. Huguenard J. R., Coulter D. A. and Prince D. A. (1991) A fast transient potassium current in thalamic relay neurons—kinetics of activation and inactivation. *J. Neurophysiol.* **66**, 1304–1315.
16. Huguenard J. R. and McCormick D. A. (1992) Simulation of the currents involved in rhythmic oscillations in thalamic relay neurons. *J. Neurophysiol.* **68**, 1373–1383.
17. Huguenard J. R. and Prince D. A. (1991) Slow inactivation of a TEA-sensitive k-current in acutely isolated rat thalamic relay neurons. *J. Neurophysiol.* **66**, 1316–1328.
18. Huguenard J. R. and Prince D. A. (1992) A novel t-type current underlies prolonged calcium-dependent burst firing in gabaergic neurons of rat thalamic reticular nucleus. *J. Neurosci.* **12**, 3804–3817.
19. Huguenard J. R. and Prince D. A. (1994) Intrathalamic rhythmicity studied *in vitro*: nominal T-current modulation causes robust antioscillatory effects. *J. Neurosci.* **14**, 5485–5502.

20. Jahnsen H. and Llinas R. (1984) Electrophysiological properties of guinea pig thalamic neurones: an *in vitro* study. *J. Physiol., Lond.* **349**, 205–226.
21. Jahnsen H. and Llinas R. (1984) Ionic basis for the electroresponsiveness and oscillatory properties of guinea-pig thalamic neurons *in vitro*. *J. Physiol., Lond.* **349**, 227–247.
22. Leresche N., Lightowler S., Soltesz I., Jassik-Gerschenfeld D. and Crunelli V. (1991) Low-frequency oscillatory activities intrinsic to rat and cat thalamocortical cells. *J. Physiol., Lond.* **441**, 155–174.
23. Llinas R. R. (1988) The intrinsic electrophysiological properties of mammalian neurons: insights into central nervous system function. *Science* **242**, 1654–1664.
24. Lytton W. W. and Sejnowski T. J. (1992) Computer model of ethosuximide's effect on a thalamic neuron. *Ann. Neurol.* **32**, 131–139.
25. McCormick D. A. (1992) Neurotransmitter actions in the thalamus and cerebral cortex and their role in neuromodulation of thalamocortical activity. *Prog. Neurobiol.* **39**, 337–388.
26. McCormick D. A. and Huguenard J. R. (1992) A model of the electrophysiological properties of thalamocortical relay neurons. *J. Neurophysiol.* **68**, 1384–1400.
27. McCormick D. A., Huguenard J. R. and Stowbridge B. W. (1991) Determination of state dependent processing in thalamus by single neuron properties and neuromodulators. In *Single Neuron Computation* (eds McKenna T., Davis J. and Zornetzer S. F.), pp. 259–290. Academic Press, New York.
28. McCormick D. A. and Pape H. C. (1990) Properties of a hyperpolarization-activated cation current and its role in rhythmic oscillation in thalamic relay neurones. *J. Physiol., Lond.* **431**, 291–318.
29. McCormick D. A. and Pape H. C. (1990) Properties of a hyperpolarization-activated cation current and its role in rhythmic oscillations in thalamic relay neurones. *J. Physiol., Lond.* **431**, 291–318.
30. Morison R. S. and Basset D. L. (1945) Electrical activity of the thalamus and basal ganglia in decorticate cats. *J. Neurophysiol.* **8**, 309–314.
31. Nunez A., Curro-Dossi R., Contreras D. and Steriade M. (1992) Intracellular evidence for incompatibility between spindle and delta oscillations in thalamocortical neurons of cat. *Neuroscience* **48**, 75–85.
32. Pare D., Dossi R. C. and Steriade M. (1991) 3 types of inhibitory postsynaptic potentials generated by interneurons in the anterior thalamic complex of cat. *J. Neurophysiol.* **66**, 1190–1204.
33. Penny G. R., Itoh K. and Diamond I. T. (1982) Cells of different sizes in the ventral nuclei project to different layers of the somatic cortex in the cat. *Brain Res.* **242**, 55–65.
34. Ralston H. J. (1983) The synaptic organization of the ventrobasal thalamus in the rat, cat and monkey. In *Somatosensory Integration in the Thalamus* (eds Macchi G., Rustioni A. and Spreafico R.), pp. 241–250. Elsevier, Amsterdam.
35. Rose R. M. and Hindmarsh J. L. (1989) The assembly of ionic currents in a thalamic neurons: I The three-dimensional model. *Proc. R. Soc. Lond. B* **237**, 267–288.
36. Soltesz I. and Crunelli V. (1992) A role for low-frequency, rhythmic synaptic potentials in the synchronization of cat thalamocortical cells. *J. Physiol., Lond.* **457**, 257–276.
37. Soltesz I., Lightowler S., Leresche N., Jassik-Gerschenfeld D., Pollard C. E. and Crunelli V. (1991) Two inward currents and the transformation of low-frequency oscillations of rat and cat thalamocortical cells. *J. Physiol., Lond.* **441**, 175–197.
38. Steriade M., Curro Dossi R. and Nunez A. (1991) Network modulation of a slow intrinsic oscillation of cat thalamocortical neurons implicated in sleep delta waves: cortically induced synchronization and brainstem cholinergic suppression. *J. Neurosci.* **11**, 3200–3217.
39. Steriade M., Deschenes M., Domich L. and Mulle C. (1985) Abolition of spindle oscillations in thalamic neurons disconnected from nucleus reticularis thalami. *J. Neurophysiol.* **54**, 1473–1497.
40. Steriade M., Domich L., Oakson G. and Deschenes M. (1987) The deafferented reticular thalamic nucleus generates spindle rhythmicity. *J. Neurophysiol.* **57**, 260–273.
41. Steriade M., Jones E. G. and Llinas R. R. (1990) *Thalamic Oscillations and Signaling*. J. Wiley, New York.
42. Steriade M. and Llinas R. R. (1988) The functional states of the thalamus and the associated neuronal interplay. *Physiol. Rev.* **68**, 649–742.
43. Steriade M., McCormick D. A. and Sejnowski T. J. (1993) Thalamocortical oscillations in the sleeping and aroused brain. *Science* **262**, 679–685.
44. Steriade M., Nunez A. and Amzica F. (1993) Intracellular analysis of relations between the slow (<1 Hz) neocortical oscillation and other sleep rhythms of the electroencephalogram. *J. Neurosci.* **13**, 3266–3283.
45. Steriade M., Nunez A. and Amzica F. (1993) A novel slow (<1 Hz) oscillation of neocortical neurons *in vivo*: depolarizing and hyperpolarizing components. *J. Neurosci.* **13**, 3252–3265.
46. Steriade M., Parent A. and Hada J. (1984) Thalamic projections of nucleus reticularis thalami of cat: a study using retrograde transport of horseradish peroxidase and fluorescent tracers. *J. comp. Neurol.* **229**, 531–547.
47. Suzuki S. and Rogawski M. A. (1989) T-type calcium channels mediate the transition between tonic and phasic firing in thalamic neurons. *Proc. natn. Acad. Sci. U.S.A.* **86**, 7228–7232.
48. Toth T. and Crunelli V. (1992) Computer simulations of the pacemaker oscillations of thalamocortical cells. *NeuroReport* **3**, 65–68.
49. von Krosigk M., Bal T. and McCormick D. A. (1993) Cellular mechanisms of a synchronized oscillation in the thalamus. *Science* **261**, 361–364.
50. Wang X. J. (1994) Multiple dynamical models of thalamic relay neurons—rhythmic bursting and intermittent phase-locking. *Neuroscience* **59**, 21–31.
51. Wang X. J., Rinzel J. and Rogawski M. A. (1991) A model of the T-type calcium current and the low-threshold spike in thalamic neurons. *J. Neurophysiol.* **66**, 839–850.